JOC*Article*

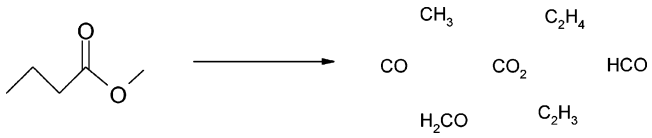
# Thermal Decomposition of Methyl Butanoate: Ab Initio Study of a Biodiesel Fuel Surrogate

Lam K. Huynh and Angela Violi*

*Department of Mechanical Engineering, The University of Michigan, Ann Arbor, Michigan 48109-2125*

*avioli@umich.edu*

*Received August 23, 2007*




In this paper, we report a detailed analysis of the breakdown kinetic mechanism for methyl butanoate (MB) using theoretical approaches. Electronic structures and structure-related molecular properties of reactants, intermediates, products, and transition states were explored at the BH&HLYP/cc-pVTZ level of theory. Rate constants for the unimolecular and bimolecular reactions in the temperature range of 300−2500 K were calculated using Rice−Ramsperger−Kassel−Marcus and transition state theories, respectively. Thirteen pathways were identified leading to the formation of small compounds such as $CH_3$, $C_2H_3$, CO, $CO_2$, and $H_2CO$. For the initial formation of MB radicals, H, $CH_3$, and OH were considered as reactive radicals participating in hydrogen abstraction reactions. Kinetic simulation results for a high temperature pyrolysis environment show that MB radicals are mainly produced through hydrogen abstraction reactions by H atoms. In addition, the $C(O)OCH_3 = CO + CH_3O$ reaction is found to be the main source of CO formation. The newly computed kinetic sub-model for MB breakdown is recommended as a core component to study the combustion of oxygenated species.

## 1. Introduction

Biofuels are liquid, solid, or gaseous fuels derived from renewable biological sources. Biomass can be burned directly for thermal energy or converted to other high value energy sources including ethanol, biodiesel, methanol, hydrogen, or methane.[1] Biodiesel is a biologically derived diesel fuel substitute created by chemically reacting vegetable oils or animal fats with an alcohol (methanol is the usual choice) to produce fatty acid methyl esters of the R−(C═O)−O−R′ form (where R and R′ are carbon chains of alkyl and alkenyl) with as many as 16−18 carbon atoms. Biodiesel is the name given to these esters when they are intended for use as fuel. Blends of up to 20% biodiesel (mixed with petroleum diesel fuels) can be used in nearly all diesel equipment and are compatible with most storage and distribution equipment.

Methyl butanoate (MB) or butyrate, $CH_3CH_2CH_2C(O)OCH_3$, has been widely used as a convenient surrogate for large biofuel methyl ester molecules in flame simulations[2−4] due to its essential chemical structural features, namely, R−C(═O)O−−$CH_3$. Little information on reaction pathways, thermodynamics, and kinetics of MB and the species derived from it, however, is available in the literature. In 2000, Fisher et al.[2] developed the first detailed chemical kinetic model for methyl butanoate. In the study, the authors analyzed the combustion of MB in closed vessels at low temperature in sub-atmospheric conditions and identified some discrepancies along with some qualitative agreements between the computed results and the experimental data. The mechanism was then modified by Gaïl et al.[3] to study the combustion of MB in a jet stirred reactor, an opposed flow diffusion flame, and a variable pressure flow reactor. Metcalfe et al.[1] modified the mechanism in an attempt to study the ignition delay data for $MB/O_2/Ar$ mixtures. The Fisher mechanism was also used as a core component for a larger kinetic model for oxygenated hydrocarbons to investigate soot emissions from diesel engines.[4] In these kinetic mechanisms, however, the rate constants for MB reactions and its derivatives were estimated using similar reactions available in the literature, and to our

* Corresponding author. Fax: (734) 647-9379.

(1) Metcalfe, W. K.; Dooley, S.; Curran, H. J.; Simmie, J. M.; Al-Nahas, A. M.; Navarro, M. V. *J. Phys. Chem. A* **2007**, *111*, 4001.

(2) Fisher, E. M.; Pits, W. J.; Curran, H. J.; Westbrook, C. K. *Proc. Combust. Inst.* **2000**, *28*, 1579−1586.

(3) Gaïl, S.; Thomson, M. J.; Sarathy, S. M.; Syed, S. A.; P. Dagaut, B.; Dievart, P.; Marchese, A. J.; Dryer, F. L. *Proc. Combust. Inst.* **2007**, *31*, 305−311.

(4) Westbrook, C. K.; Pitz, W. J.; Curran, H. J. *J. Phys. Chem. A* **2006**, *110*, 6912−6922.

10.1021/jo701824n CCC: $40.75 © 2008 American Chemical Society
Published on Web 12/04/2007

best knowledge, such rate constant assignments have not been systematically validated.

In this paper, we report a detailed analysis of the breakdown mechanism of MB using electronic structure and chemical kinetics calculations. After a section describing the methodology, results are presented for 13 kinetic pathways leading to the formation of small hydrocarbons.

## 2. Computational Methods

All of the electronic structure calculations were carried out using the Gaussian 03 program.[5] A hybrid nonlocal density functional theory (DFT), namely, Becke's half-and-half (BH&H)[6] nonlocal exchange and the Lee−Yang−Parr (LYP)[7] nonlocal correlation functionals, was used to explore the potential energy surface (PES) for the identified important pathways of MB breakdown. This level of theory has been found to be sufficiently accurate for predicting the transition state properties for hydrogen abstraction reactions by radicals[8−10] (e.g., hydrogen abstraction reactions by H, OH, and $CH_3$ radicals), which were considered in this study to form MB radicals by breaking the C−H bond (cf. Discussion). This level of theory has been widely used to study hydrogen abstraction reactions from hydrocarbons.[11−18] The geometry and frequency calculations for all of the species were carried out using Dunning's correlation-consistent polarized valence triple-ζ basis set denoted as cc-pVTZ,[19] which is believed to be sufficient to capture physical changes along the reaction coordinate for the reactions studied. Normal analyses were performed to verify the nature of the stationary points (reactants, intermediates, and products). For species having more than one conformation, the lowest energy conformation was considered. Transition states were identified by the existence of singular imaginary frequencies. To confirm a transition state for several complicated reactions, the minimum energy path from reactants to products passing through the transition state was also calculated using the intrinsic reaction path (IRC).[20,21]

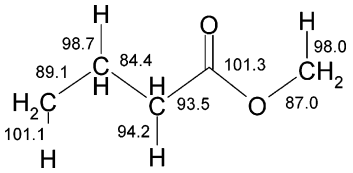



**FIGURE 1.** CBS-QB3 computed bond energies for MB (kcal/mol).[30]

All rate constants were calculated employing the kinetic module of the web-based Computational Science and Engineering Online (CSE-Online) environment.[22] The Rice−Ramsperger−Kassel−Marcus (RRKM) theory and the canonical transition state theory methods[23−25] were used to derive high pressure limit rate constants for unimolecular and bimolecular reactions, respectively. The tunneling effect was included in the rate constants using the one-dimensional Eckart methodology.[26] Hindered rotation corrections for certain low frequency modes (e.g., the rotation of $CH_3$ and $C_2H_5$ groups along the C−C bond) are also incorporated in the calculated rate constants using the approach proposed by Ayala and Schlegel.[27] This formalism optimizes the accuracy for treating a single rotor to minimize the compound errors in the case of multiple internal rotors. To calculate the hindered rotation correction factor for a certain vibrational mode to the partition function, the vibrational mode, the rotating group, as well as the periodicity number of the torsional potential must be identified. From the given information together with the geometry of the molecule of interest, information needed for calculating the correction factor of hindered rotation treatment (e.g., reduced moment of inertia and the periodic potential) can be obtained. The correction factor is then calculated using a fitting formula (ref 27, eq 26), which was derived from the tabulated accurate values to improve upon Pitzer et al.'s formula.[28,29] The fitting formula retains the positive characteristics of Pitzer et al.'s formula for high $V_0/kT$ while improving its behavior for low $V_0/kT$, where $V_0$ is the internal rotation barrier height.

Discretely calculated values of rate constants for a reaction at different temperatures were fitted into the modified Arrhenius expression as $k(T) = AT^n \exp(-E_a/RT)$ in the temperature range of 300−2500 K.

## 3. Results and Discussion

**3.1. Initiation Step.** In high temperature regimes, MB can decompose by either unimolecular reactions or bimolecular hydrogen abstraction reactions. Figure 1 shows the calculated bond dissociation energies for MB using the CBS-QB3 level of theory.[30]

If the unimolecular reaction proceeds through a simple fission (one bond breaking at a time), the $C_2H_5-CH_2C(O)OCH_3$ bond has the lowest dissociation energy of ∼85 kcal/mol. If the reaction goes through a complex fission (multiple bonds break

(5) Frisch, M. J.; Trucks, G. W.; Schlegel, H. B.; Scuseria, G. E.; Robb, M. A.; Cheeseman, J. R.; Montgomery, J. A., Jr.; T. V.; Kudin, K. N.; Burant, J. C.; Millam, J. M.; Iyengar, S. S.; Tomasi, J.; Barone, V.; Mennucci, B.; Cossi, M.; Scalmani, G.; Rega, N.; Petersson, G. A.; Nakatsuji, H.; Hada, M.; Ehara, M.; Toyota, K.; Fukuda, R.; Hasegawa, J.; Ishida, M.; Nakajima, T.; Honda, Y.; Kitao, O.; Nakai, H.; Klene, M.; Li, X.; Knox, J. E.; Hratchian, H. P.; Cross, J. B.; Adamo, C.; Jaramillo, J.; Gomperts, R.; Stratmann, R. E.; Yazyev, O.; Austin, A. J.; Cammi, R.; Pomelli, C.; Ochterski, J. W.; Ayala, P. Y.; Morokuma, K.; Voth, G. A.; Salvador, P.; Dannenberg, J. J.; Zakrzewski, V. G.; Dapprich, S.; Daniels, A. D.; Strain, M. C.; Farkas, O.; Malick, D. K.; Rabuck, A. D.; Raghavachari, K.; Foresman, J. B.; Ortiz, J. V.; Cui, Q.; Baboul, A. G.; Clifford, S.; Cioslowski, J.; Stefanov, B. B.; Liu, G.; Liashenko, A.; Piskorz, P.; Komaromi, I.; Martin, R. L.; Fox, D. J.; Keith, T.; Al-Laham, M. A.; Peng, C. Y.; Nanayakkara, A.; Challacombe, M.; Gill, P. M. W.; Johnson, B.; Chen, W.; Wong, M. W.; Gonzalez, C.; Pople, J. A. *Gaussian 03, Revision A.1*; Gaussian, Inc.: Pittsburgh, PA, 2003.

(6) Becke, A. D. *J. Chem. Phys.* **1993**, *98*, 1372−1377.

(7) Lee, C.; Yang, W.; Parr, R. G. *Phys. Rev. B* **1988**, *37*, 785−789.

(8) Truong, T. N.; Duncan, W. *J. Chem. Phys.* **1994**, *101*, 7408−7414.

(9) Lynch, B. J.; Fast, P. L.; Harris, M.; Truhlar, D. G. *J. Phys. Chem. A* **2000**, *104*, 4811−4815.

(10) Zhang, Q.; Bell, R.; Truong, T. N. *J. Phys. Chem. A* **1995**, *99*, 592−599.

(11) Violi, A.; Truong, T. N.; Sarofim, A. F. *J. Phys. Chem. A* **2004**, *108*, 4846.

(12) Huynh, L. K.; Ratkiewicz, A.; Truong, T. N. *J. Phys. Chem. A* **2006**, *110*, 473−484.

(13) Huynh, L. K.; Zhang, S.; Truong, T. N. *Combust. Flame* **2007**, in press.

(14) Huynh, L. K.; Truong, T. N. *Theor. Chem. Acc.* **2007**, in press.

(15) Chae, K.; Violi, A. *J. Org. Chem.* **2007**, *72*, 3179−3185.

(16) Wang, D.; Violi, A. *J. Org. Chem.* **2006**, *71*, 8365−8371.

(17) Wang, D.; Violi, A.; Kim, D. H.; Mullholland, J. A. *J. Phys. Chem. A* **2006**, *110*, 4719−4725.

(18) Violi, A. *J. Phys. Chem. A* **2005**, *109*, 7781−7787.

(19) Dunning, T. H. J. *J. Chem. Phys.* **1989**, *90*, 1007−1023.

(20) Gonzalez, C.; Schlegel, H. B. *J. Chem. Phys.* **1989**, *90*, 2154−2161.

(21) Gonzalez, C.; Schlegel, H. B. *J. Phys. Chem.* **1990**, *94*, 5523−5527.

(22) Truong, T. N.; Nayak, M.; Huynh, H. H.; Cook, T.; Mahajan, P.; Tran, L.-T. T.; Bharath, J.; Jain, S.; Pham, H. B.; Boonyasiriwat, C.; Nguyen, N.; Andersen, E.; Kim, Y.; Choe, S.; Choi, J.; Cheatham, T. E., III; Facelli, J. C. *J. Chem. Inf. Model.* **2006**, *46*, 971−984.

(23) Glasstone, S.; Laidler, K. J.; Eyring, H. *The Theory of Rate Processes*; McGraw-Hill: New York, 1941.

(24) Truhlar, D. G.; Garrett, B. C.; Klippenstein, S. J. *J. Phys. Chem.* **1996**, *100*, 12771.

(25) Forst, W. *Theory of Unimolecular Reactions*; Academic Press: New York, 1973.

(26) Miller, W. H. *J. Am. Chem. Soc.* **1979**, *101*, 6810−6814.

(27) Ayala, P. Y.; Schlegel, H. B. *J. Chem. Phys.* **1998**, *108*, 2314.

(28) Pitzer, K. S.; Gwinn, W. D. *J. Chem. Phys.* **1942**, *10*, 428−440.

(29) Li, J. C. M.; Pitzer, K. S. *J. Phys. Chem.* **1956**, *60*, 466−474.

(30) El-Nahas, A. M.; Navarro, M. V.; Simmie, J. M.; Joseph, W. Bozzelli; Curran, H. J.; Dooley, S.; Metcalfe, W. *J. Phys. Chem. A* **2007**, *111*, 3727−3739.




**FIGURE 2.** Four MB radicals formed by breaking a C−H bond: (a) radical **1a**, $CH_2CH_2CH_2C(O)OCH_3$; (b) radical **2a**, $CH_3CHCH_2C(O)OCH_3$; (c) radical **3a**, $CH_3CH_2CHC(O)OCH_3$; and (d) radical **4a**, $CH_3CH_2CH_2C(O)OCH_2$.

and form at the same time), the lowest barrier path has a barrier of ∼70 kcal/mol to form $C_2H_4 + CH_2C(OH)OCH_3$.[30] On the contrary, if the initiation reaction is a bimolecular hydrogen abstraction reaction by reactive flame radicals such as H, OH, and $CH_3$, the reaction has a rather low barrier. For example, the abstraction reaction between MB and H to form the four initial radicals (see Figure 2) has an average reaction barrier of 7.3 kcal/mol. Therefore, of the two types of initial reactions, the bimolecular routes can be dominant in conditions where reactive radicals are abundant. In this study, we focus our effort on the initial step caused by the hydrogen abstraction reactions between MB and flame radicals H, OH, and $CH_3$.

The barrier height values of the hydrogen abstraction reactions at a specific site depend on the type of attacking radicals. Particularly, if the radical is $CH_3$ (methyl radical), the reaction has an average barrier height of 15.5 kcal/mol. Reactions with OH and H have lower values of about 4.3 and 7.3 kcal/mol, respectively. Because of the similarity of these reactions and for simplicity, only the reaction of MB with a H atom is considered in the next sections. However, rate constants for reactions between MB and other two radicals (OH and $CH_3$) were also calculated, and the results are reported in the Supporting Information.

The BH&HLYP/cc-pVTZ level of theory is used to explore the PES of the MB breakdown mechanism. Since we are interested in the initiation reaction of hydrogen abstraction by flame radicals, this level of theory is an excellent choice that compromises the cost and the accuracy for predicting the transition state properties for hydrogen abstraction reactions by radicals.[8−10] To gain more confidence in the performance of the DFT, we first computed the heat of formation of MB at 298 K, $\Delta H^\circ_{f,289K}$ (MB), using the two following isodesmic/isogyric reactions:

$$CH_3CH_2CH_2C(O)OCH_3 + CH_3CHO \rightarrow CH_3C(O)OCH_3 + CH_3CH_2CH_2CHO \quad (R_1)$$

$$CH_3CH_2CH_2C(O)OCH_3 + CH_3OH \rightarrow CH_3C(O)OCH_3 + CH_3CH_2CH_2OH \quad (R_2)$$

In an isodesmic reaction, the type of chemical bonds broken in the reactant are the same as the type of bonds formed in the reaction product; thus, this type of reaction is often used as a hypothetical reaction in thermochemistry, especially in calculating the heat of formation of a species. It is known that the heat of formation for a species can be obtained using isodesmic reactions with higher accuracies than using the atomization methods due to cancellation of errors including those from the thermodynamic contributions from hindered rotors, which can be difficult to compute. These two reactions have been previously used by El-Nahas et al.[30] to calculate the heat of formation of MB at the CBS-QB3 level of theory.

Table 1 reports the available heats of formation for the species involved in reactions $R_1$ and $R_2$. Using these values, our calculations yield $\Delta H^\circ_{f,289K}$ (MB) = −107.80 and −108.34 kcal/mol for reactions $R_1$ and $R_2$, respectively.

**TABLE 1. Heat of Formation $\Delta H^\circ_{f,289K}$ (kcal/mol) for Species Used in Isodesmic Reactions $R_1$ and $R_2$**

| species | $\Delta H^\circ_{f,289K}$ | ref |
|---|---|---|
| $CH_3OH$ | −48.06 ± 0.05 | 35 |
| $CH_3CHO$ | −39.70 ± 0.12 | 36 |
| $CH_3C(O)OCH_3$ | −98.83 ± 0.29 | 37 |
| $CH_3CH_2CH_2OH$ | −60.97 | 38 |
| $CH_3CH_2CH_2CHO$ | −48.85 ± 0.33 | 39 |

These data give an averaged value of −108.06 kcal/mol, which is in excellent agreement with values present in the literature. Liu and Cheng[31] analyzed a set of 35 straight-chained alkyl carboxylic acids and esters and determined their atomization energies from DFT and ab initio calculations together with known heats of formation. They computed the heat of formation for MB at different levels of theory and obtained a value of −108.60 kcal/mol using the B3LYP/6-311++G(3df,-2pd)//B3LYP/4-31G(d) method and −108.91 kcal/mol at the MP2/6-31+G(d)//HF/4-31G(d) level of theory. El-Nahas et al. estimated a value of 108.60 kcal/mol at the CBS-QB3 level of theory.

**3.2. Propagation Steps.** The four initial radicals (cf. Figure 2) formed by breaking the C−H bond can either undergo isomerization or break down to form smaller compounds through $\beta$-scission reactions. Because the bond energy of the C−H bond is larger than that of the C−C bond, the latter is more likely to be broken in $\beta$-scission reactions. In some cases, where there is no C−C bond available, breaking the C−H bond is the only way to create smaller species. Because of the large number of propagated reactions involved in the MB breakdown, we limit this study to certain pathways that are feasible as well as chemically important. The final products of these reaction pathways are chosen to be common species in flames such as $CO_2$, CO, $H_2CO$, $CH_3$, $C_2H_3$, and $C_2H_4$. We envision that these reaction pathways could be incorporated into existing mechanisms easily and consistently. The 13 reaction pathways explored in this study are schematically presented in Figure 3.

The four initial MB radicals **1a**, **2a**, **3a**, and **4a** formed by hydrogen abstraction reactions are shown in Figure 2. These radicals can isomerize through hydrogen migration reactions. For example, radical **1a** can be converted to radicals **2a**, **3a**, and **4a** (and vice versa) through 1−2, 1−3, and 1−6 hydrogen migration reactions. Similarly, radical **2a** can become **3a** and **4a** through 1−2 and 1−5 hydrogen migration reactions, respectively. The 1−4 hydrogen migration is responsible for the transformation between radicals **3a** and **4a**. Figure 4 shows the barrier heights for these reactions, ranging from 29 to 42 kcal/mol.

The energy barriers depend on the type of hydrogen migration. If the reaction proceeds through a transition state having a low ring constraint energy (e.g., seven-membered ring for the

(31) Liu, M. H.; Cheng, S.-R. *J. Mol. Struct.* **2006**, *763*, 149−154.

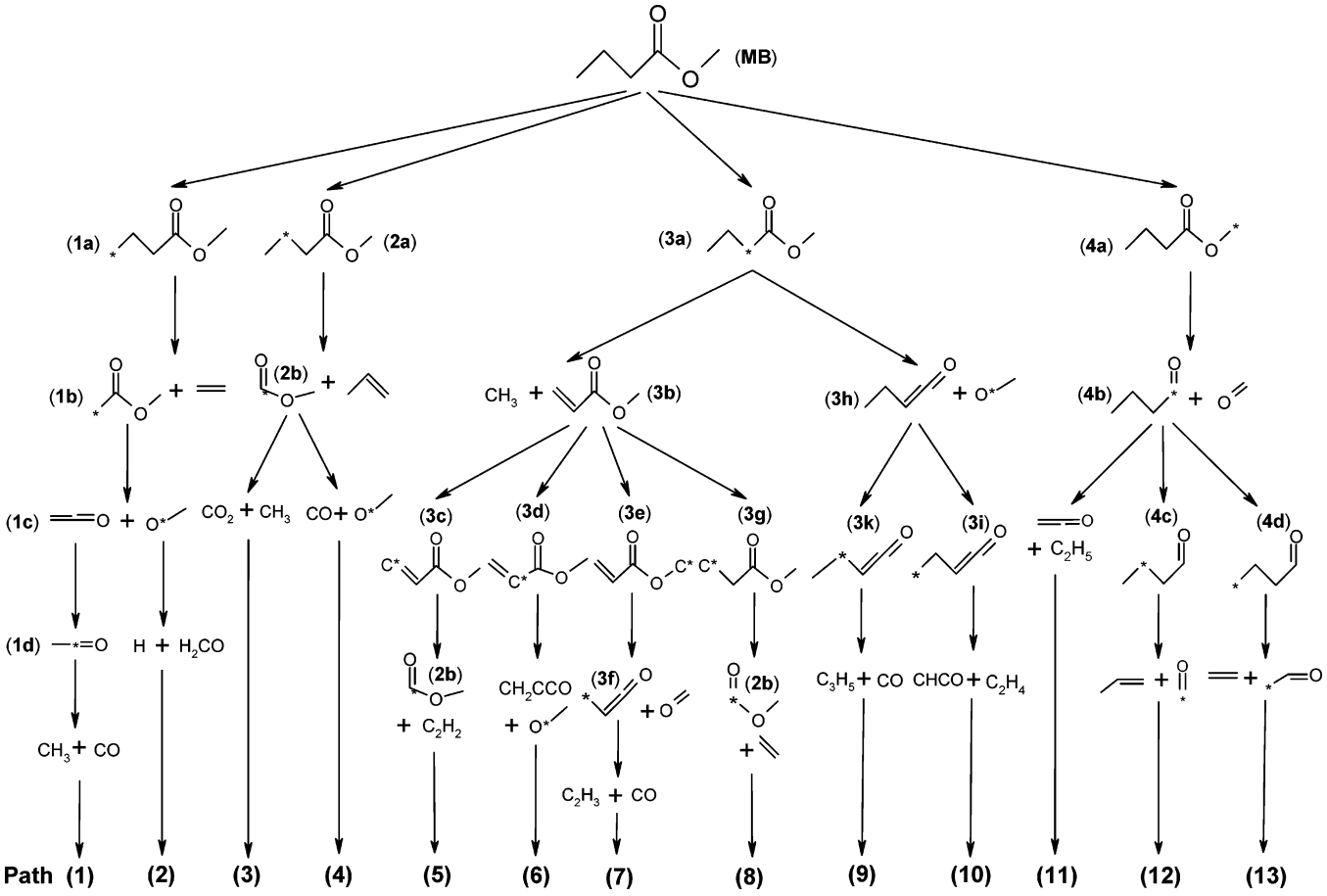



**FIGURE 3.** Explored reaction pathways for MB breakdown initiated by hydrogen abstraction reactions.

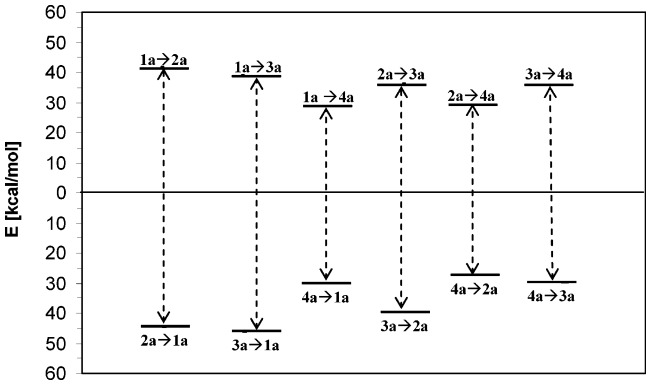



**FIGURE 4.** Barrier heights for isomerization reactions among initial radicals: **1a**, **2a**, **3a**, and **4a** (cf. Figure 2). The notation **1a** → **2a** denotes the transition state from **1a** to **2a**.

1−6 hydrogen migration reaction), the barrier height is lower than that of a transition state involving a four-membered ring (e.g., 1−3 hydrogen migration). This explains the decreasing trend of barrier heights in the order of 1−2, 1−3, and 1−4 hydrogen migration. The same trend is found for the reverse barrier heights (e.g., **3a** → **1a** and **3a** → **2a** for the 1−3 and 1−2 hydrogen migrations, respectively).

**3.2.1. Pathways 1 and 2.** Radical **1a**, $CH_2CH_2CH_2C(O)OCH_3$ (cf. Figure 2a), is formed from MB by a hydrogen abstraction reaction by a hydrogen atom with a barrier height of 8.3 kcal/mol. The barrier heights for the hydrogen abstraction reactions at the same site by radicals OH and $CH_3$ are 5 and 17 kcal/mol, respectively. Through $\beta$-scission, the radical decomposes to form $C_2H_4$ (ethylene) and $CH_2C(O)OCH_3$ (**1b**) that eventually breaks down into small species, $CH_3O$ and $CH_2CO$, through C−C bond cleavage with a high energy barrier of 49 kcal/mol. The C−H scission of intermediate $CH_3O$ can form $H_2CO$ (acetaldehyde) and a H atom with a high barrier height of 31.6 kcal/mol. From $CH_2CO$, CO and $CH_3$ are then produced through H addition followed by $\beta$-scission at the C−C bond. Energetic profiles for these pathways are given in Figure 5.

**3.2.2. Pathways 3 and 4.** Figure 6 reports the energy profiles for reaction pathways 3 and 4. Radical **2a**, $CH_3CHCH_2C(O)OCH_3$ (cf. Figure 2b), is formed by an abstraction reaction with an energy barrier lower (6.5 kcal/mol) than the one to form **1a**. Radical **2a** then decomposes through a $\beta$-scission reaction to form $C_3H_6$ (propylene) and $C(O)OCH_3$ (**2b**). Intermediate **2b** can form CO + $CH_3O$ and $CO_2$ + $CH_3$ by breaking the C−O and C−C bonds, respectively. Because the bond energy of C−O is higher than that of C−C (∼86 and 83 kcal/mol, respectively), the second product channel ($CO_2$ + $CH_3$) has a lower barrier of 16.6 kcal/mol as compared to 20.8 kcal/mol to produce CO + $CH_3O$.

More confidence in the choice of the DFT method used in this study can be gained by performing a close analysis of the energetic data of the $C(O)OCH_3$ (**2b**) = $CO_2$ + $CH_3$ reaction (cf. reaction pathway 3 in Figure 6). Even though the energies of the cis and trans conformations of the $C(O)OCH_3$ radical are the same, the transition state coming from the cis conformation has a much lower energy than that from the trans

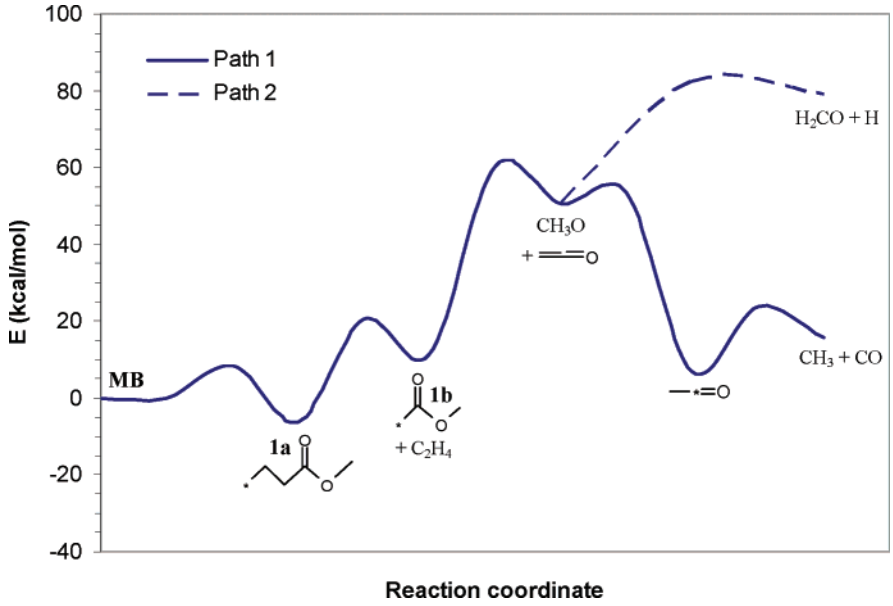



**FIGURE 5.** Energetic profiles for reaction pathways 1 and 2. Zero-point energy corrections are included.

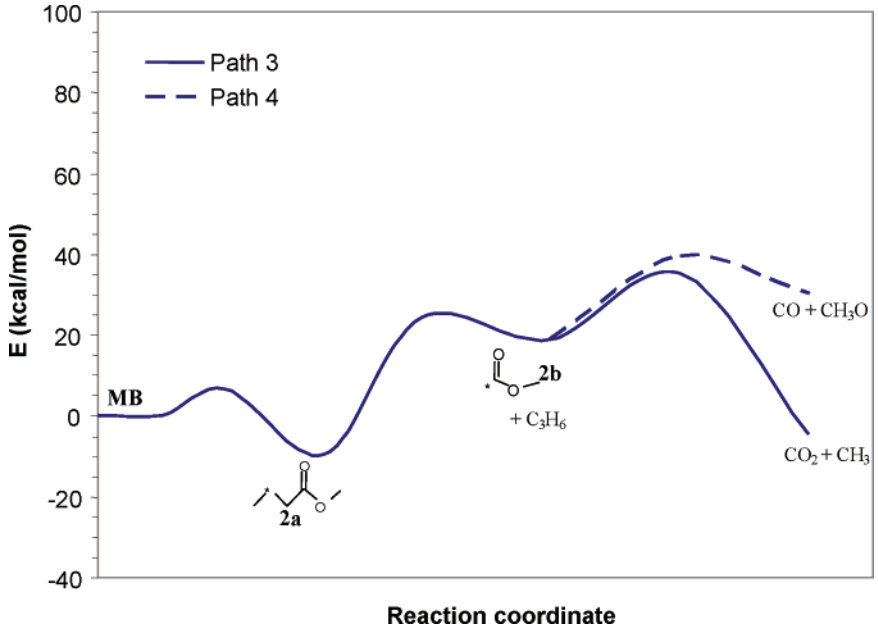



**FIGURE 6.** Energetic profiles for reaction pathways 3 and 4. Zero-point energy corrections are included.

conformation.[32] Therefore, in this study, we only consider the cis conformation. The computed barrier height (with the zero-point energy correction) is 16.3 kcal/mol, which agrees well with the ~14.5 kcal/mol literature value obtained at the high level of theory G3//B3LYP and CCSD(T)/aug-cc-pV(Q+d)Z//CCSD(T)/6-311G(2df,p) methods. The calculated reaction energy of 23.4 kcal/mol for this reaction is also in good agreement with the literature data, particularly the values of 22.9 kcal/mol at QCISD(T)/6-311++G(3df,3pd)[33] and 23.5 kcal/mol at G3//B3LYP.[32] In addition, the DFT optimized geometries for the reactants and transition state are very consistent with those obtained using a high level of theory.[32]

**3.2.3. Pathways 5−8.** Figure 7 shows the energetic profiles for reaction pathways 5−8. These four product channels (reaction pathways) are produced from the same intermediate $CH_2CHC(O)OCH_3$ (**3b**) that is formed by breaking the C−C bond of $CH_3CH_2CHC(O)OCH_3$ (**3a**) through a $\beta$-scission reaction.

Radicals $CHCHC(O)OCH_3$ (**3c**), $CH_2CC(O)OCH_3$ (**3d**), and $CH_2CHC(O)OCH_3$ (**3e**) can be obtained by hydrogen abstraction from **3b** at different reaction sites. These radicals can isomerize through hydrogen migration reactions. Radical **3c** can produce $C_2H_2$ and $CH_3C(O)O$ (intermediate **2b** as in Figure 5) by C−C bond cleavage, while **3d** can lead to $CH_3O$ and $CH_2CCO$. Radical **3e** can decompose to $H_2CO$ and $CH_2CHCO$ (**3f**), which produces $C_2H_3$ and CO. If an H atom is added to intermediate **3b** at the carbon next to the carbonyl group, the radical **3g** is

(32) McCunn, L. R.; Lau, K.-C.; Krisch, M. J.; Butler, L. J.; Tsung, J.-W.; Lin, J. J. *J. Phys. Chem. A* **2006**, *110*, 1625−1634.
(33) Francisco, J. S. *Chem. Phys.* **1998**, *237*, 1.

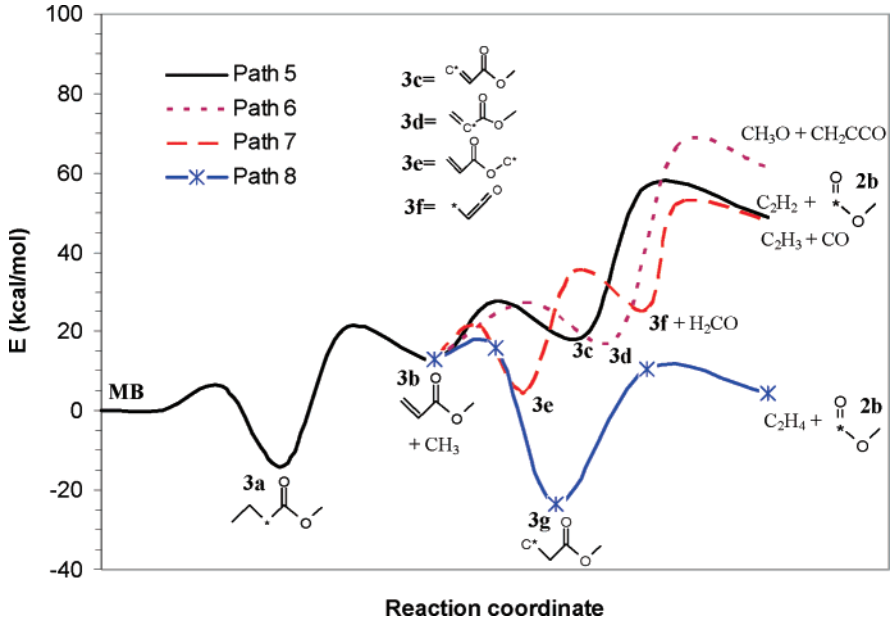



**FIGURE 7.** Energetic profiles for reaction pathways 5−8. Zero-point energy corrections are included.

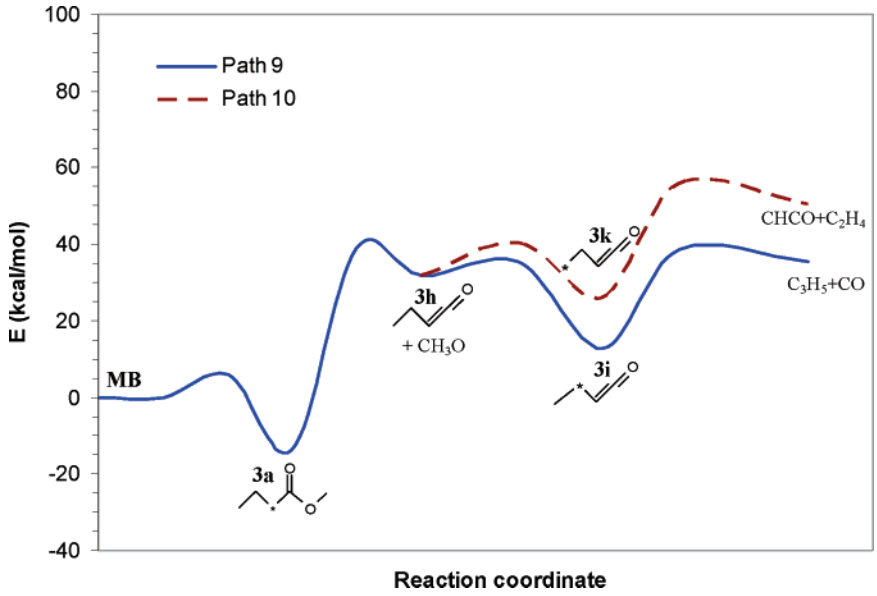



**FIGURE 8.** Energetic profiles for reaction pathways 9 and 10. Zero-point energy corrections are included.

formed. This reaction has been previously identified as one of the main routes in the oxidation of MB in a jet stirred reactor, an opposed flow diffusion flame, and a variable pressure flow reactor.[3] From **3g**, $C_2H_4$ and **2b** are produced by C−C bond fission with a barrier height of 34.1 kcal/mol. Intermediate **2b** produced from **3c** (pathway 5) and **3g** (pathway 8) can decompose to form $CO_2$ + $CH_3$ and CO + $CH_3O$ through pathways 3 and 4, respectively (cf. Figure 6).

**3.2.4. Pathways 9 and 10.** Alternatively, radical **3a** can form $CH_3O$ and $CH_3CH_2CHCO$ (**3h**) by breaking the C−O bond, instead of the C−C bond as in Figure 7. As expected, this $\beta$-scission reaction has a higher barrier than the previous one (52.9 kcal/mol as compared to 34.3 kcal/mol) due to the strong C−O bond. Intermediate **3h** can form $CH_2CH_2CHCO$ (**3k**) and $CH_2CHCHCO$ (**3i**) through hydrogen abstractions by reactive radicals in flames. Figure 8 shows energetic profiles where the attacking radical is a H atom. Radicals **3k** and **3i** can decompose to produce CHCO + $C_2H_4$ and $C_3H_5$ + CO, respectively.

**3.2.5. Pathways 11−13.** Radical $CH_3CH_2CH_2C(O)OCH_2$ (**4a**) can form intermediate $CH_3CH_2CH_2CO$ (**4b**) and $CH_2O$ by breaking the C−O bond. Radical **4b** can then lead to $C_2H_5$ + $CH_2CO$ (pathway 11) or isomerize to form $CH_3CHCH_2CO$ (**4c**) and $CH_2CH_2CH_2CO$ (**4d**) through 1−3 and 1−4 hydrogen migrations, respectively. Radicals **4c** and **4d** decompose to $C_3H_6$ + CHO and $C_2H_4$ + $CH_2CHO$ by C−C bond cleavage, respectively. The relative energies (to reactant) of $C_2H_5$ + $CH_2$-CO and $C_2H_4$ + $CH_2CHO$ are the same, even though they have different barrier heights. Radical $CH_2CHO$ can form the stable species $CH_2CO$ by breaking the C−H bond through a $\beta$-scission reaction with a high barrier height of 47 kcal/mol. This gives a relative energy of 86 kcal/mol. If $CH_2CO$ is formed by hydrogen abstraction, the barrier height is much lower, being ∼4.3 kcal/

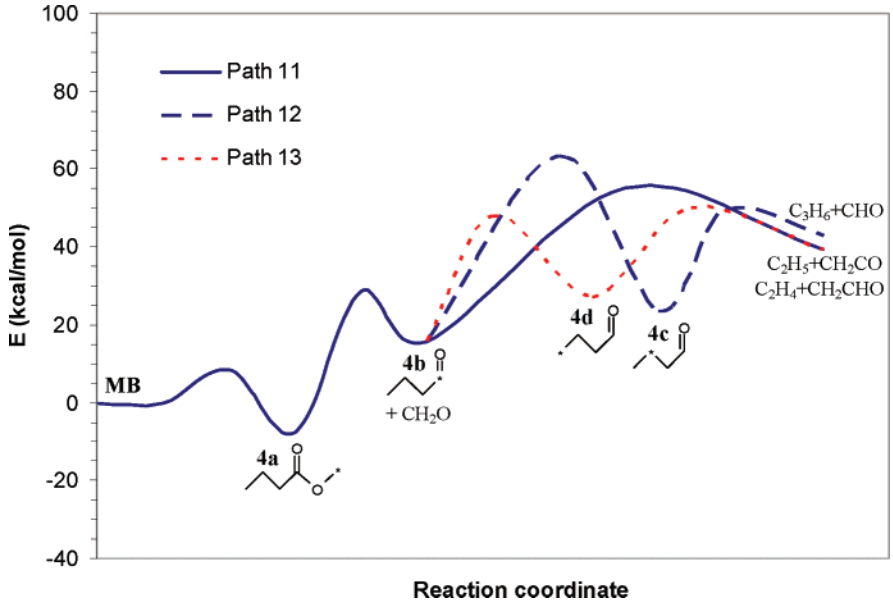



**FIGURE 9.** Energetic profiles for reaction pathways 11−13. Zero-point energy corrections are included.

mol. However, there is a surface crossing between the triplet state (reactants) and singlet state (products) surface for this reaction. For this reason, in this work, we do not consider this possibility. The energetic profiles for reaction pathways 11−13 are given in Figure 9.

The optimized structures and frequencies of all the species identified are calculated at the BH&HLYP/cc-pVTZ level of theory and are reported in Supporting Information Tables S1−and S2.

**3.3. Kinetic Calculations.** Using DFT potential energy surfaces together with the geometries and frequencies of reactants, intermediates, transition states, and products, we computed the rate constants for the unimolecular and bimolecular reactions identified in the previous section. The corrections for tunneling and hindered rotation treatment were included in the calculations. The rate constants were then fitted to a modified Arrhenius expression as $k(T) = AT^n \exp(-E_a/RT)$, given in Supporting Information Tables S3−S6.

**3.4. Reaction Mechanism and Kinetic Modeling.** The 13 reaction pathways for MB breakdown and their corresponding reaction rate constants were implemented in a kinetic model analysis. We employed the CHEMKIN 4.1 software package[34] to study the time evolution of a closed homogeneous reacting gas mixture system at conditions of general combustion applications (1 atm and 700−1500 K). Although this is not a complete kinetic model for MB pyrolysis, qualitative conclusions can be drawn from such an analysis. Particularly, the relative importance of the bimolecular hydrogen abstraction reactions in the initiation stage and the temperature dependence of small hydrocarbons such as $C_2H_2$ through the analysis of the $CO/CO_2$ ratio at different temperatures can be obtained.

**TABLE 2. Normalized Rate-of-Consumption Coefficients of Bimolecular Initiation Reactions for MB at Several Temperatures[a]**

| | reaction | temp (K) 700 | 800 | 1000 | 1200 | 1500 |
|---|---|---|---|---|---|---|
| $R_3$ | MB + H = **1a** + $H_2$ | 0.090 | 0.106 | 0.128 | 0.143 | 0.157 |
| $R_4$ | MB + H = **2a** + $H_2$ | 0.252 | 0.252 | 0.240 | 0.225 | 0.204 |
| $R_5$ | MB + H = **3a** + $H_2$ | 0.236 | 0.224 | 0.202 | 0.184 | 0.164 |
| $R_6$ | MB + H = **4a** + $H_2$ | 0.091 | 0.108 | 0.136 | 0.158 | 0.185 |
| | total MB + H reaction | 0.670 | 0.690 | 0.706 | 0.710 | 0.710 |
| $R_7$ | MB + $CH_3$ = **1a** + $CH_4$ | 0.090 | 0.106 | 0.128 | 0.143 | 0.157 |
| $R_8$ | MB + $CH_3$ = **2a** + $CH_4$ | <0.001 | <0.001 | <0.001 | <0.001 | <0.001 |
| $R_9$ | MB + $CH_3$ = **3a** + $CH_4$ | <0.001 | <0.001 | <0.001 | <0.001 | <0.001 |
| $R_{10}$ | MB + $CH_3$ = **4a** + $CH_4$ | <0.001 | <0.001 | <0.001 | <0.001 | <0.001 |
| | total MB + $CH_3$ reaction | 0.090 | 0.106 | 0.128 | 0.143 | 0.157 |
| $R_{11}$ | MB + OH = **1a** + $H_2O$ | 0.058 | 0.052 | 0.044 | 0.039 | 0.034 |
| $R_{12}$ | MB + OH = **2a** + $H_2O$ | 0.086 | 0.063 | 0.039 | 0.028 | 0.020 |
| $R_{13}$ | MB + OH = **3a** + $H_2O$ | 0.061 | 0.054 | 0.045 | 0.040 | 0.035 |
| $R_{14}$ | MB + OH = **4a** + $H_2O$ | 0.036 | 0.037 | 0.039 | 0.040 | 0.043 |
| | total MB + OH reaction | 0.241 | 0.206 | 0.167 | 0.147 | 0.132 |

[a] Analysis was carried out at the initial stage ($t$ = 0 s). The normalized rate-of-consumption coefficient of a reaction is obtained by normalizing the corresponding absolute rate-of-consumption coefficient, which is calculated by taking the product of (rate constant)[MB][R], where R = H, $CH_3$, or OH. The notations **1a**, **2a**, **3a**, and **4a** denote the abstraction products as presented in Figure 2.

Table 2 shows the analysis of normalized rate-of-consumption coefficients of hydrogen abstraction reactions at the initiation stage of MB breakdown. The reaction between H and MB is found to be the main consumption source of the reactant (MB) in the temperature range of 700−1500 K, even though at 0 K it does not have the lowest barrier height (7.3 kcal/mol as compared to 4.3 kcal/mol of the lowest energy barrier reaction, OH + MB; cf. Initiation Step).

The same conclusion can be drawn by examining the magnitude of the calculated rate constants for these reactions in the same temperature range (see Tables S3−S6 in the Supporting Information). The observation can be explained by the difference in the total free energy $\Delta G^{\ddagger}(T) = \Delta H^{\ddagger}(T) -$

(34) Kee, R. J.; F. M. R.; Miller, J. A.; Coltrin, M. E.; Grcar, J. F.; Meeks, E.; Moffat, H. K.; Lutz, A. E.; Dixon-Lewis, G.; Smooke, M. D.; Warnatz, J.; Evans, G. H.; R. S. L.; Mitchell, R. E.; Petzold, L. R.; Reynolds, W. C.; Caracotsios, M.; Stewart, W. E.; Glarborg, P.; Wang, C.; McLellan, C. L.; Adigun, O.; W. G. H.; Chou, C. P.; Miller, S. F.; Ho, P.; Young, P. D.; Young, D. J.; Hodgson, D. W.; Petrova, M. V.; Puduppakkam, K. V. *CHEMKIN Release 4.1*; San Diego, CA, 2006.
(35) Green, J. H. S. *Chem. Ind. (London)* **1960**, 1215−1216.
(36) Pedley, J. B.; Naylor, R. D.; Kirby, S. P. *Thermochemical Data of Organic Compounds*, 2nd ed.; Chapman and Hall: London, 1986.
(37) Verevkin, S. P.; Beckhaus, H.-D.; Belen'kaja, R. S.; Rakus, K.; Ruchardt, C. *Thermochim. Acta* **1996**, *279*, 47−64.
(38) Luo, Y.-R.; Kerr, J. A. In *CRC Handbook of Chemistry and Physics*, 86th ed.; Lide, D. R., Ed.; CRC Press: Boca Raton, FL, 2005.
(39) Buckley, E.; Cox, J. D. *Trans. Faraday Soc.* **1967**, *63*, 895−901.

**TABLE 3. Mol Fraction Ratio of $CO_2$ to CO and Normalized Rate-of-Production Coefficient of Reactions for CO Formation at Several Temperatures[a]**

| | | temp (K) | | | | |
|---|---|---|---|---|---|---|
| | reaction | 700 | 800 | 1000 | 1200 | 1500 |
| | $CO + CO_2$ (mol fraction) | $3.8 \times 10^{-3}$ | $3.72 \times 10^{-3}$ | $3.6 \times 10^{-3}$ | $3.37 \times 10^{-3}$ | $3.19 \times 10^{-3}$ |
| | $CO_2/CO$ | 53.4 | 35.5 | 20.4 | 14.2 | 10.0 |
| | Contribution of reactions to CO formation | | | | | |
| $R_{15}$ | $CH_3CO = CO + CH_3$ | 0.283 | 0.182 | 0.141 | 0.104 | 0.080 |
| $R_{16}$ | $C(O)OCH_3 = CO + CH_3O$ | 0.668 | 0.775 | 0.827 | 0.869 | 0.895 |
| $R_{17}$ | $CH_2CHCO = CO + C_2H_3$ | 0.050 | 0.043 | 0.032 | 0.027 | 0.024 |
| $R_{18}$ | $CH_3CH_2CHCO = CO + C_3H_5$ | <0.001 | <0.001 | <0.0001 | <0.001 | <0.001 |

[a] Values are computed at 5% consumption of MB.

$T\Delta S^{\ddagger}(T)$ at the transition state (relative to that of the reactants) among the reactions, which governs changes of rate constants with temperature. In other words, the thermal corrections to the rate constants are not the same for the three kinds of hydrogen abstraction reactions.

The total contribution of the H + MB reaction to the fuel consumption increases with temperature. For example, the total rate-of-consumption coefficients of this type of reaction are 0.67 and 0.71 at 700 and 1500 K, respectively. The coefficients of the $CH_3$ + MB reaction trend upward, while those of the OH + MB reaction can be seen to have a downward trend (cf. Table 2). Therefore, it is expected that at low temperatures, the coefficient for OH + MB will be greater than that of H + MB, which is consistent with the potential energy surface at 0 K.

Of the four reactions between MB and H (cf. $R_3-R_6$ in Table 2), reaction $R_4$ to form radical **2a**, $CH_3CHCH_2C(O)OCH_3$, is the most important reaction in consuming MB in the considered temperature range, even though at 0 K this reaction has a higher barrier than that of reaction $R_5$ to form **3a**, $CH_3CH_2CHC(O)OCH_3$ (6.5 and 6.0 kcal/mol for $R_4$ and $R_5$, respectively). As the temperature increases, the contribution of reaction $R_6$ to the fuel consumption becomes more significant than that of reaction $R_5$, which is the second most important at temperatures lower than 1400 K.

For the MB + H system, we analyzed the total mol fraction of CO + $CO_2$ at several temperatures (see Table 3). The total mol fraction of CO + $CO_2$ decreases with temperature. The pathways producing CO and $CO_2$ are thermodynamically favorable, having lower energies as compared to the others (cf. Figures 5−9). Thermodynamically, these channels dominate at low temperature regime. When the temperature increases, the system gains more energy, and additional pathways become available.

Table 3 also presents the ratio of $CO_2$ to CO. This ratio decreases as the temperature increases. There are two and one oxygen (O) atoms in $CO_2$ and CO, respectively; thus, the decrease of the $CO_2/CO$ ratio suggests that the O fraction increases in other products. In other words, the fraction of C remaining in the form of a soot precursor decreases with a decrease of the $CO_2/CO$ ratio.

In the kinetic model, CO can be formed by the four final reactions, reactions $R_{15}-R_{18}$. Table 3 also shows the analysis of the normalized contribution of each reaction to the formation of CO. Reaction $R_{16}$ is mainly responsible for the formation of CO for the whole temperature range, while reaction $R_{18}$ contributes least to CO production. Note that CO can be produced by complex channels that go through the four final reactions; thus, the contribution of each channel can be explained by both the difference in the barrier heights and the length (the number of elementary reactions involved) and/or the manifold (the number of parallel channels involved) of each product channel. For example, CO and $CO_2$ were both produced through intermediate **2b** ($C(O)OCH_3$), whose concentration is determined by reactions $R_{19}$ (pathway 3), $R_{20}$ (pathway 5), and $R_{21}$ (pathway 7)

$$CH_3CHCH_2C(O)OCH_3 = C_3H_6 + C(O)OCH_3 \quad (R_{19})$$

$$CHCHC(O)OCH_3 = C_2H_2 + C(O)OCH_3 \quad (R_{20})$$

$$CH_2CH_2C(O)OCH_3 = C_2H_4 + C(O)OCH_3 \quad (R_{21})$$

For a complete picture of MB pyrolysis, it is therefore important to incorporate the MB reactions into existing kinetic schemes for flame combustion and pyrolysis to improve the prediction of important species concentrations.

## 4. Conclusions

The reaction pathways and kinetics of the breakdown mechanism for MB were explored using theoretical approaches. Electronic structures and other related molecular properties of the species involved in the reaction pathways were explored at the BH&HLYP/cc-pVTZ level of theory. The rate constants for all elementary reactions in the temperature range of 300−2500 K were calculated using RRKM and transition state theory methodology. Thirteen reaction pathways were identified, and the kinetic sub-model for the MB breakdown was then used to derive the relative importance of bimolecular hydrogen abstraction reactions by different reactive radicals (H, OH, and $CH_3$). The H + MB reaction was found to be the most important reaction in the initial stage of MB breakdown. The $C(O)OCH_3 = CO + CH_3O$ reaction was the main source of CO formation. The computed kinetic sub-model for MB breakdown is recommended to be embedded into existing kinetic models to study the combustion of MB as well as other related oxygenated species.

**Acknowledgment.** This research was funded by the Air Force Scientific Office for Research (Grant FA9550-06-1-0376) and the Office of Naval Research (Grant F017146).

**Supporting Information Available:** Tables of optimized geometries and calculated frequencies of all species and transition states at the BH&HLYP/cc-pVTZ level of theory together with tables of calculated RRKM and transition state theory rate constants for all studied reactions. This material is available free of charge via the Internet at http://pubs.acs.org.

JO701824N